

Enhancing urban CFD simulations with porous media parameters for representative street trees

Junghyeon Ahn^{a,b}, Junsuk Kang^{a,c,d,*}

^a Department of Civil and Environmental Engineering, Seoul National University, Seoul 08826, Republic of Korea

^b JH Solution Co., Ltd., No.1701, 135 Gasan digital 2-40, Geumcheon-gu, Seoul 08504, Republic of Korea

^c Research Institute of Agriculture and Life Sciences, Seoul National University, Seoul 08826, Republic of Korea

^d Department of Landscape Architecture and Rural Systems Engineering, Seoul National University, Seoul 08826, Republic of Korea

ARTICLE INFO

Keywords:

Porous resistance coefficient
Street trees
Urban CFD simulation
Vegetation modeling
Aerodynamic validation

ABSTRACT

This study presents a computational fluid dynamics (CFD)-based approach for extracting and validating flow resistance values for six major street tree species commonly found in urban environments. To simplify the modeling process while retaining aerodynamic accuracy, complex tree geometries were replaced with porous media regions in numerical wind tunnel simulations. Pressure drop data across a range of inlet velocities (1–20 m/s) were used to derive species-specific resistance coefficients through second-order polynomial fitting.

The extracted coefficients were validated by comparing the pressure drop profiles of the porous models with those of full-scale tree models, showing strong agreement (coefficient of determination $R^2 \approx 0.9999$) and less than 5% error at higher velocities. The results also revealed that aerodynamic resistance is more closely related to canopy morphology—such as leaf area, shape, and volume fraction—than to leaf density alone.

This method provides a practical and scalable solution for incorporating vegetation effects into urban airflow simulations, significantly reducing computational costs. The findings offer a useful framework for integrating species-specific tree characteristics into urban environmental planning and design, including applications in urban ventilation analysis, pollution dispersion modeling, and green infrastructure planning.

1. Introduction

The urban street trees are essential components of green infrastructure that provide a wide range of ecological and climatic benefits, including shade provision, microclimate regulation, air pollution mitigation, and carbon sequestration (Escobedo et al., 2011; McPherson et al., 1994; Nowak et al., 2006). In dense urban areas, trees serve not only aesthetic and ecological functions but also contribute significantly to the modification of local air flow patterns, temperature distributions, and particulate matter dispersion (Grimmond and Oke, 1999). Accordingly, there has been growing attention to the integration of vegetation effects in urban environmental simulations, particularly those employing computational fluid dynamics (CFD).

In CFD-based modeling of urban microclimates, the aerodynamic and thermal effects of trees are increasingly recognized as critical variables. To accurately predict wind flows and pollutant transport in urban canyons, it is essential to account for vegetation-induced drag, wake formation, and turbulence modulation within the canopy layer (Amorim

et al., 2013; Hong et al., 2018; Kim and Kang, 2023). Trees can obstruct or redirect airflow in complex ways, often leading to localized increases or reductions in pollutant concentrations depending on spatial configuration, species characteristics, and seasonal canopy density (Baek et al., 2024). As such, trees have become indispensable modeling elements in urban-scale CFD studies.

Despite this recognized importance, many existing CFD simulations represent trees using highly simplified approaches. Common practices include modeling vegetation as porous blocks with uniform resistance or applying empirical drag functions based on leaf area density (LAD) (Manickathan et al., 2018). While these approaches reduce computational cost, they fail to capture the heterogeneous and species-dependent morphology of real trees. This oversimplification can result in significant prediction errors, particularly in simulations involving sensitive applications such as pedestrian comfort, air quality forecasting, and ventilation design.

Vegetation, moreover, is not merely a passive aerodynamic obstruction; it behaves as a dynamic biological system that interacts

* Corresponding author.

E-mail address: junkang@snu.ac.kr (J. Kang).

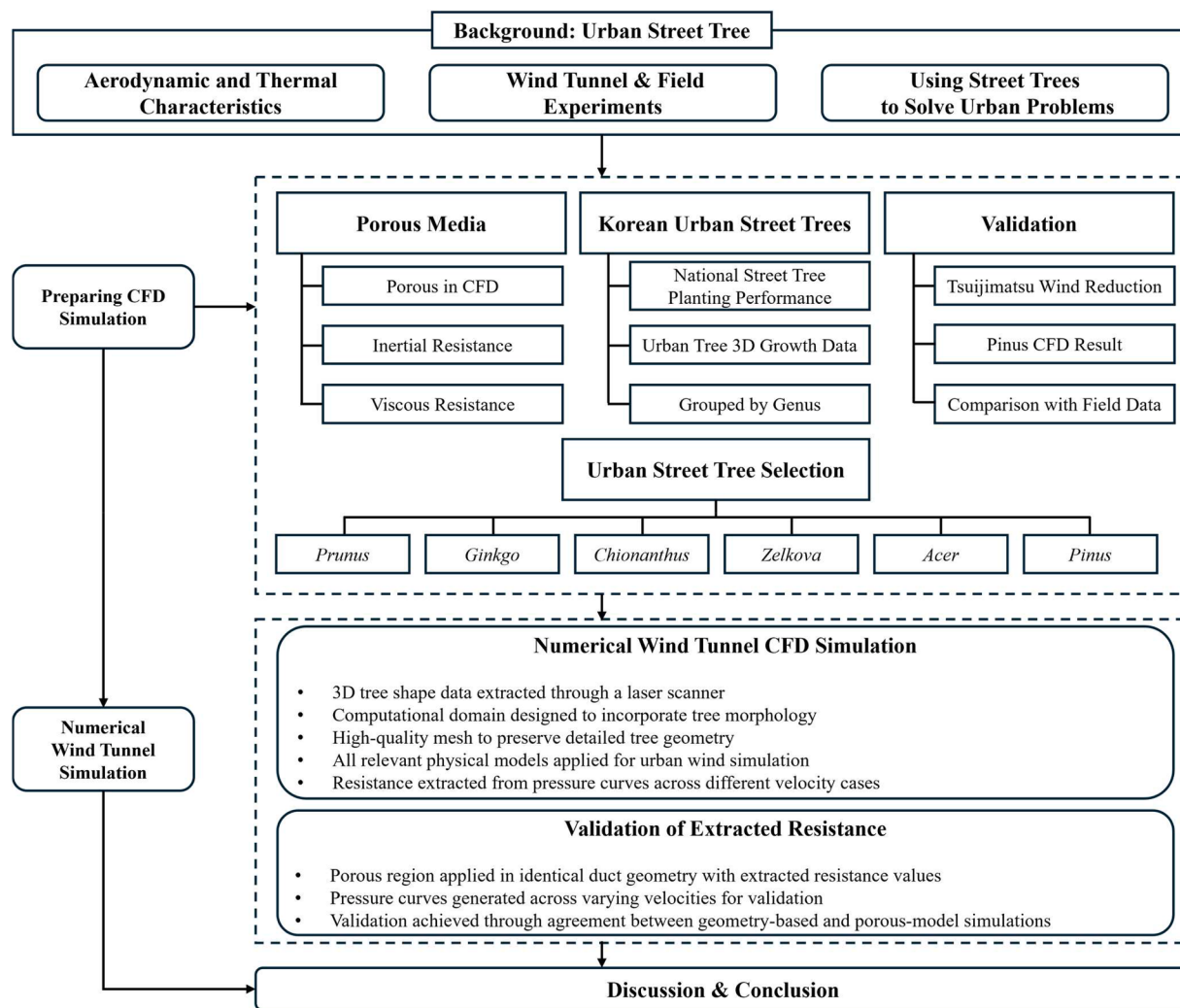


Fig. 1. Schematic sequence of study structure.

Table 1

Total number of the most frequently planted street tree species in South Korea based on the 2020 national inventory (Korea Forest Service, 2020).

Species	Total Number of Trees
<i>Prunus</i> subg. <i>Cerasus</i>	552,872
<i>Prunus</i> × <i>yedoensis</i>	1008,020
<i>Ginkgo biloba</i>	1029,695
<i>Zelkova serrata</i>	543,614
<i>Metasequoia glyptostroboides</i>	179,154
<i>Platanus occidentalis</i>	247,328
<i>Acer palmatum</i>	215,008
<i>Acer buergerianum</i>	95,871
<i>Liriodendron tulipifera</i>	37,036
<i>Lagerstroemia indica</i>	405,308
<i>Chionanthus retusus</i>	655,119
<i>Pinus thunbergia</i>	115,244
<i>Hibiscus syriacus</i>	507,257
Others	3831,303
Total	9442,829

with wind through flexible branches and reconfiguring canopies (De Langre, 2008). Although CFD techniques have advanced considerably, there remains a notable gap between the availability of high-resolution modeling tools and their application to accurate, species-specific tree representation in urban contexts. Bridging this gap requires a robust methodology for quantifying tree-induced drag properties in a form

compatible with scalable CFD simulations. As a practical solution, this study adopts a porous media-based modeling approach that simplifies complex tree geometries into resistance-defined volumes. This method enables species-specific aerodynamic effects to be captured while maintaining computational efficiency in urban-scale CFD. Previous research has demonstrated that such porous approaches can effectively reproduce the bulk aerodynamic influence of vegetation (Moonen et al., 2012; Santiago et al., 2007).

In urban contexts, where several tens to hundreds of trees are often present, explicitly resolving detailed branch-leaf structures are computationally prohibitive. The porous media approach provides a tractable alternative that preserves the dominant aerodynamic effects relevant for wind flow, ventilation, and microclimate analysis. Although small-scale turbulence interactions within the canopy are inevitably smoothed out, this limitation is outweighed by the practical benefits of scalability and efficiency. Furthermore, by extracting species-specific resistance coefficients and validating them against both detailed tree models and measurement data, this study strengthens the applicability of the method for real-world urban CFD applications.

To address these limitations, this study aims to extract porous media resistance parameters—specifically, inertial and viscous resistance coefficients—for six street tree species commonly planted in South Korea. Using 3D tree models derived from detailed geometry data, we conduct high-resolution virtual wind tunnel simulations for each species and derive flow resistance values based on pressure loss and turbulence

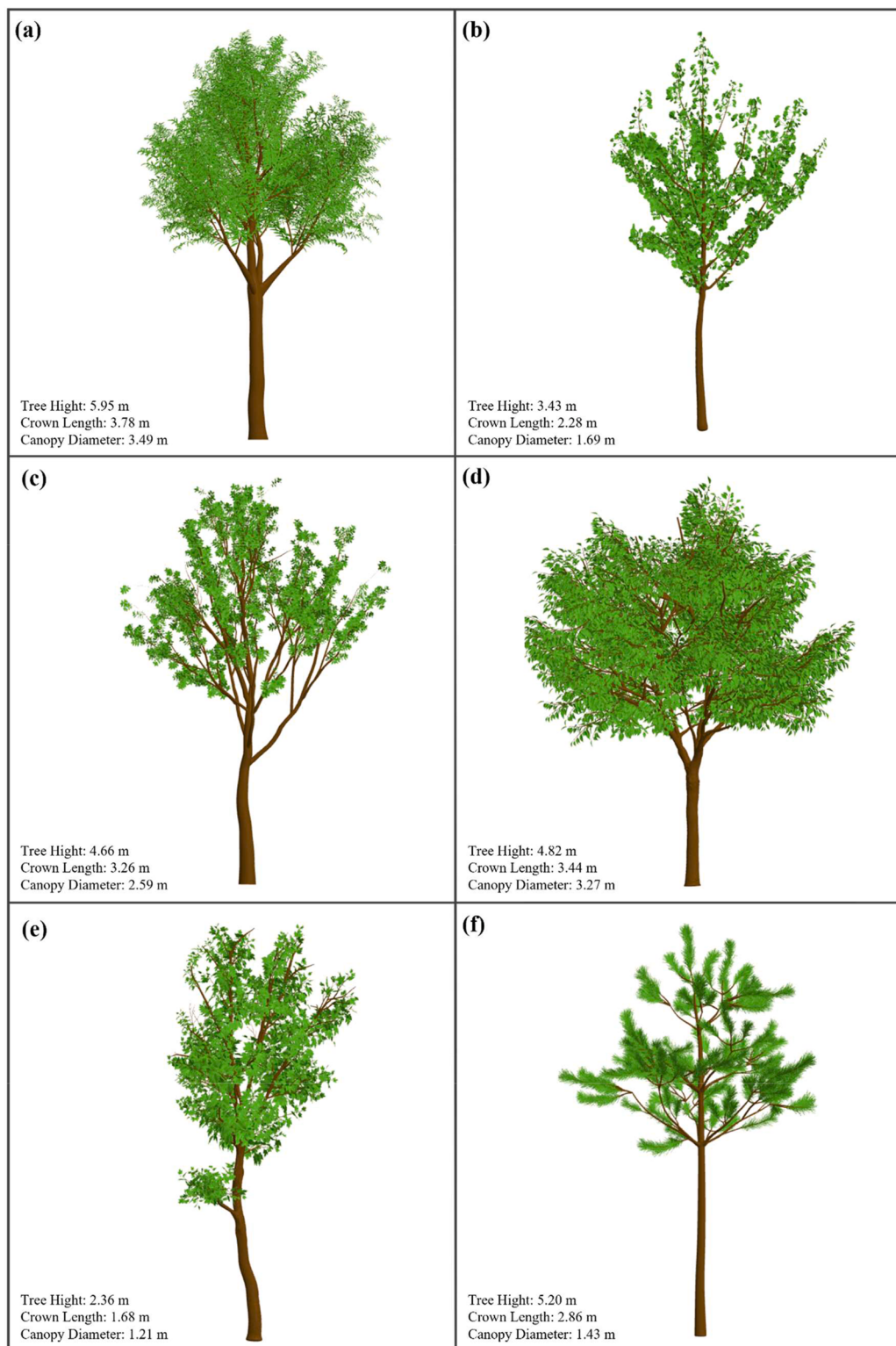


Fig. 2. Representative 3D tree geometries with annotated morphological parameters selected by genus: (a) *Prunus*, (b) *Ginkgo*, (c) *Chionanthus*, (d) *Zelkova*, (e) *Acer*, (f) *Pinus* ([Ministry of Science and ICT, 2023](#)).

characteristics. These results are then translated into porous media inputs applicable to urban-scale CFD models. To ensure the reliability of these parameters, validation was performed using field-based aerodynamic data from Japanese black pine (*Pinus thunbergii*) windbreak forests. By systematically parameterizing aerodynamic resistance across representative tree species, the study offers a practical reference for incorporating realistic vegetation effects in broader urban

environmental assessments.

2. Literature review

Urban vegetation, particularly trees, plays a significant role in modifying local air flow and influencing the dispersion of air pollutants in built environments. Numerous studies have demonstrated that

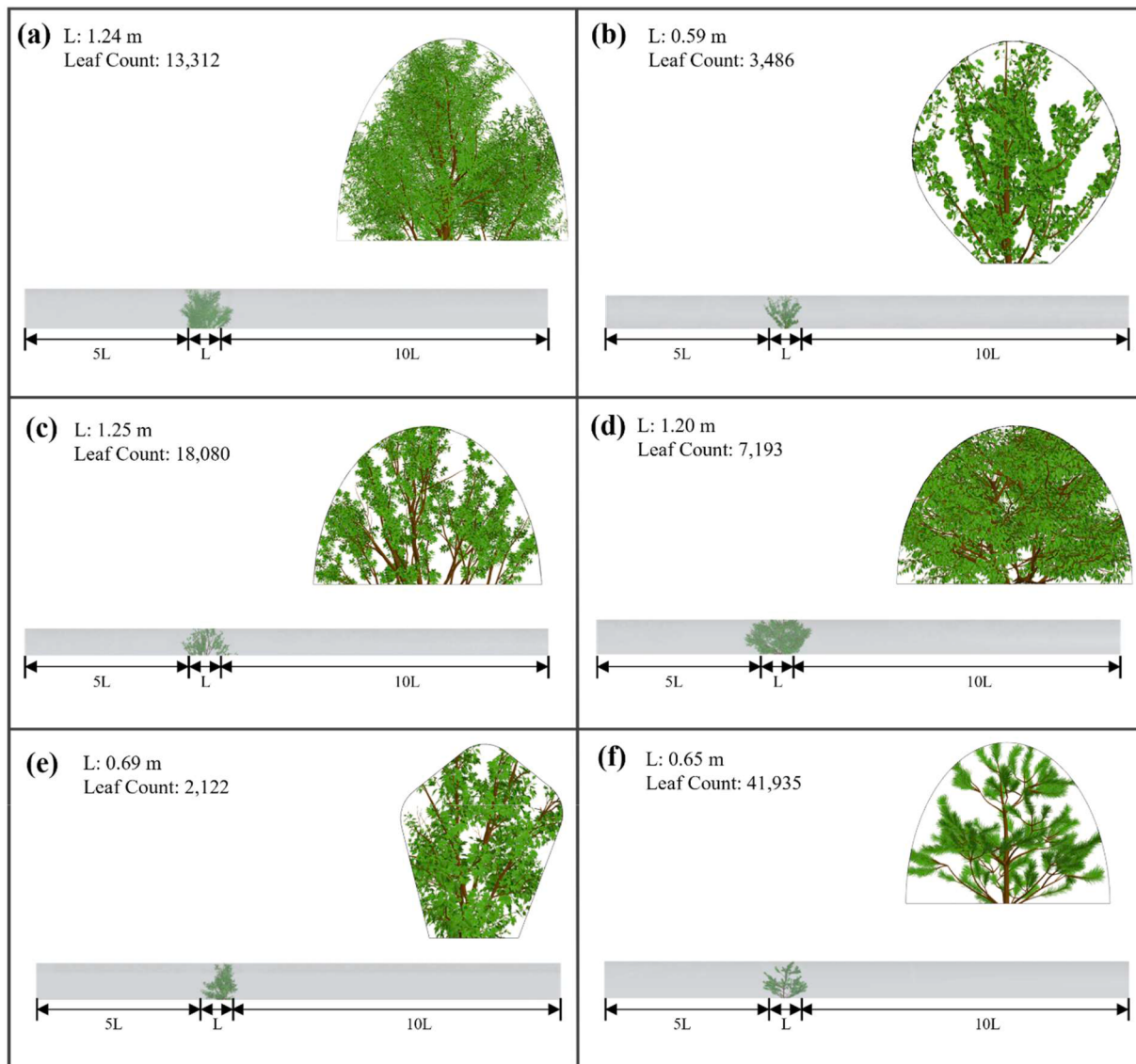


Fig. 3. Numerical wind tunnel geometry for the six representative tree models with domain dimensions and tree placement. Cross-sectional views of each tree species are also shown: (a) *Prunus*, (b) *Ginkgo*, (c) *Chionanthus*, (d) *Zelkova*, (e) *Acer*, (f) *Pinus*.

vegetation within urban canyons can significantly affect the aerodynamic and thermal characteristics of the microclimate. [Grimmond and Oke \(1999\)](#) analyzed urban surface forms and highlighted how vegetation alters aerodynamic roughness and turbulence profiles. [Gromke and Ruck \(2007\)](#) experimentally showed that street trees can either trap or ventilate pollutants depending on their spatial arrangement. Similarly, [Buccolieri et al. \(2010\)](#) examined the implications of tree-lined streets for pollutant removal and thermal comfort, emphasizing the importance of species-specific modeling in complex urban morphologies.

Wind tunnel and field experiments have contributed significantly to understanding the aerodynamic behavior of trees. [Rudnicki et al. \(2004\)](#) measured drag coefficients and crown streamlining effects for conifer species, while [Cao et al. \(2012\)](#) demonstrated how the structural traits of shrubby trees influence flow separation and pressure drop. [Zhang et al. \(2022\)](#) investigated how fruit tree morphology and aerodynamic performance changes under operational airflow conditions, and [Ren et al. \(2023\)](#) provided in situ evidence of wind-dependent variability in canopy porosity and drag forces.

Computational fluid dynamics (CFD) has become a central tool for modeling vegetation-airflow interactions with increasing detail and

scalability. [Sogachev and Panferov \(2006\)](#) modified two-equation turbulence models to incorporate vegetation drag effects. [Manickathan et al. \(2018\)](#) compared CFD simulations of model and natural trees, highlighting the geometric simplification's impact on drag prediction. [Amani-Beni et al. \(2023\)](#) introduced high-resolution 3D tree models to investigate species-specific aerodynamic responses, emphasizing the value of precise morphological representation. [Baek et al. \(2024\)](#) employed a finite volume method-based CFD framework to assess the performance of green infrastructure in reducing PM10 concentrations in port-adjacent neighborhoods. Recently, data-driven and AI-assisted CFD approaches have emerged to enhance the scalability and adaptability of environmental simulations. [Ahn et al. \(2025\)](#) proposed a deep learning-assisted CFD methodology for analyzing thermal performance in urban areas using nature-based design strategies, representing a new generation of hybrid modeling efforts in urban environmental analysis.

Despite these developments, many urban-scale CFD studies continue to represent trees using highly simplified models, such as porous blocks or empirical drag coefficients based on leaf area density (LAD) ([Gromke and Ruck, 2008; Liu et al., 2018](#)). While these simplifications offer computational efficiency, they often overlook the aerodynamic heterogeneity of actual tree structures, leading to potential inaccuracies in

Table 2
Numerical wind tunnel simulation mesh parameters.

Surface Wrapper		
Base Size	0.1 m	
Contact Prevention	Surfaces	Branch, Leaf
- One Group Contact Prevention Set	Minimum Size	0.0001 m
Custom Controls	Part Surface	Branch, Truck, Leaf
- Surface Control	Minimum Surface Size	0.5 % Relative to base (0.0005 m)
	Target Surface Size	5.0 % Relative to base (0.005 m)
Automated Mesh		
Base Size	0.2 m	
Prism Layer Total Thickness	20.0 % Relative to base (0.04 m)	
Custom Controls	Part Surface	Wrapped surface: Branch, Truck, Leaf
- Surface Control	Minimum Surface Size	1.0 % Relative to base (0.0002 m)
	Target Surface Size	10.0 % Relative to base (0.02 m)
	Prism Layer Total Thickness	5.0 % Relative to base (0.01 m)

simulating urban air flow and pollutant dispersion. Moreover, the lack of species-specific resistance parameters limits the applicability of CFD results to real-world vegetation scenarios. To overcome these limitations, there is a growing need for refined vegetation modeling techniques that can extract aerodynamic resistance properties—such as inertial and viscous resistance—from high-resolution CFD simulations. This study addresses this gap by systematically quantifying porous media parameters for commonly planted urban street tree species, thereby providing transferable inputs for scalable and realistic urban CFD simulations.

3. Methods

3.1. Workflow

The overall research workflow is illustrated in Fig. 1. The first stage involves simulation preparation and background analysis to determine an effective method for representing urban street trees in CFD. A literature review identified the porous media approach as a computationally efficient strategy. However, few studies have addressed the process of extracting appropriate porous resistance values specifically for tree structures. Accordingly, this stage included a review of porous media formulations and an assessment of their applicability to general CFD workflows.

To establish representative tree types, commonly planted urban street trees in Korea were selected using a 3D tree dataset. Trees were categorized by genus, and six species were selected: *Prunus*, *Ginkgo*, *Chionanthus*, *Zelkova*, *Acer*, and *Pinus*.

The second stage focuses on the extraction and validation of porous resistance values through numerical wind tunnel simulations. Tree geometry was obtained via 3D laser scanning, and a computational domain was constructed to preserve morphological fidelity. High-quality mesh was generated to resolve the detailed structure of the trees, and the physical models typically used in urban wind environment simulations were applied to the numerical wind tunnel CFD. Resistance values were extracted by analyzing pressure curves under varying inlet velocity conditions.

For validation, the extracted resistance was applied to a porous region within an identical duct geometry. Resulting pressure curves were compared with those from a geometry-based simulation using the same tree model. The level of agreement between these two simulation types was used to confirm the reliability of the derived porous parameters.

Finally, all results were synthesized to draw overall conclusions. Species-specific resistance characteristics were analyzed to identify

differences in aerodynamic behavior across the selected urban street trees.

3.2. Porous media

In this study, to represent momentum loss in a simplified and computationally efficient manner, a porous media model is adopted. Rather than explicitly resolving the internal geometry of obstacles—which is computationally prohibitive in most CFD applications—the porous region is treated as a bulk volume that exerts resistance on the flow. This approach provides a practical alternative for representing flow resistance without requiring high-resolution structural modeling (Moonen et al., 2012; Santiago et al., 2007).

The governing equations for incompressible turbulent flow are based on the Reynolds-Averaged Navier–Stokes (RANS) formulation. The momentum conservation equation, including the porous media source term, is given as (Siemens PLM Software, 2023):

$$\frac{\partial \rho}{\partial t} + \nabla \cdot (\rho \mathbf{u}) = 0 \quad (1)$$

$$\rho \left(\frac{\partial u_i}{\partial t} + \frac{u_j \partial u_i}{\partial x_j} \right) = - \frac{\partial p}{\partial x_i} + \mu \frac{\partial^2 u_i}{\partial x_j^2} - (\alpha u_i + \beta |u| u_i) \quad (2)$$

where ρ is the fluid density, μ is the dynamic viscosity, p is the pressure, \mathbf{u} is velocity vector, u_i , u_j is the velocity component in the i and j directions, and α and β are the inertial and viscous resistance coefficients, respectively. This equation provides the overall computational framework for the simulations performed in this study.

In porous media modeling, the Darcy–Forchheimer equation is commonly used to describe flow resistance in porous materials (Darcy, 1856; Forchheimer, 1901). The corresponding momentum sink is added to the Navier–Stokes equations in the form:

$$S_i = - \left(\mu \frac{C_f}{d^2} u_i + \frac{1}{2} \rho \cdot C_d \cdot |u| \cdot u_i \right) \quad (3)$$

where d is a representative characteristic length, and C_f and C_d are empirical coefficients for viscous and inertial resistance, respectively. While this formulation offers a physically rigorous description, it is often difficult to apply in practice due to the complexity of parameter estimation (Gromke and Ruck, 2009; Milliez and Carissimo, 2007).

To facilitate implementation, many commercial CFD solvers adopt a simplified version of the porous media model using two empirical coefficients: viscous resistance (β) and inertial resistance (α). The corresponding momentum sink term is expressed as:

$$S_i = -(\beta \cdot u_i + \alpha \cdot |u| \cdot u_i) \quad (4)$$

where:

- β [kg/(m³·s)]: represents viscous resistance, linearly related to velocity and associated with internal friction and permeability.
- α [kg/m⁴]: represents inertial resistance, increasing nonlinearly with velocity and reflecting form drag and flow separation.

This formulation enables efficient representation of flow resistance through porous domains while maintaining reasonable physical fidelity in CFD simulations.

In practice, the resistance coefficients α and β must be determined empirically to reflect the flow resistance characteristics of the porous domain. This is typically achieved through wind tunnel experiments, where a porous sample is subjected to a range of inlet velocities and the corresponding pressure drop across the sample is measured. A pressure–velocity curve is then constructed, and the coefficients are obtained by fitting the simplified porous media formulation to the observed data. These empirically derived values serve as input parameters for the



Fig. 4. Numerical wind tunnel volume mesh for selected tree models: (a) *Prunus*, (b) *Ginkgo*, (c) *Chionanthus*, (d) *Zelkova*, (e) *Acer*, (f) *Pinus*.

momentum sink term in CFD simulations.

3.3. Korean urban street tree

According to the nationwide street tree inventory published by the Korea Forest Service (Korea Forest Service, 2022), approximately 9.42 million street trees had been planted across South Korea as of that year. Table 1 presents the species distribution, showing that although the composition varies by region due to differences in climate, local policy, and urban planning strategies, the most planted trees overall are *Prunus × yedoensis*, *Ginkgo biloba*, *Chionanthus retusus*, *Prunus* subg. *Cerasus*, and *Zelkova serrata*, in descending order of frequency. Table 1 Total number of the most frequently planted street tree species in South Korea

To facilitate research and development in digital urban modeling, the Ministry of Science and ICT has released a dataset of 320 urban tree objects through its AI Hub platform (Ministry of Science and ICT, 2023). The dataset provides laser-scanned 3D shape data in FBX format, which can serve as foundational visualization assets for digital twin platforms, machine learning model training, and environmental simulations. The

data encompasses 29 different species, multiple seasonal representations, and five distinct geographical regions, thereby reflecting diverse tree morphologies observed in Korean urban environments.

Based on the national street tree planting records, six representative species were selected for this study, each corresponding to a commonly used genus in urban streetscapes. These models were chosen to reflect typical morphological characteristics and regional prevalence and are shown in Fig. 2.

Each selected genus offers distinct advantages as urban street trees. *Prunus* (e.g., *P. × yedoensis*) is widely appreciated for its seasonal blossoms and ornamental value. *Ginkgo* (*G. biloba*) is highly resistant to urban pollution and pests, making it suitable for high-traffic areas. *Chionanthus* (notably *C. retusus*) and *Zelkova* (*Z. serrata*) are favored for their moderate size, aesthetic form, and stable canopy structure. *Acer* species provide vibrant autumn foliage, enhancing seasonal landscape diversity. *Pinus* (e.g., *P. thunbergii*), a native conifer, is frequently planted in coastal or windy regions due to its high tolerance to salinity and strong winds.

Table 3
Physical model of numerical wind tunnel simulation.

Physics Model	Description
Three Dimensional	Designed for modeling in three-dimensional mesh environments.
Steady	Compatible with separate flow and energy models for time-independent analysis.
Gradients	Allows customization of gradient computation methods.
Solution Interpolation	Provides various interpolation methods for solution data
Air	Sets air as the working fluid with standard thermophysical properties
Constant Density	Assumes incompressible flow by treating fluid density as constant
Segregated Flow	Solve mass and momentum conservation equations sequentially.
Reynolds-Averaged Navier-Stokes	Provides equations for modeling average flow rates in turbulent flow.
Realizable k-ε Turbulence	Computes turbulent kinetic energy and dissipation to model turbulence.
Two-Layer All y+ Wall Treatment	Adapts models to resolve low and high y^+ regions based on mesh resolution.
Cell Quality Remediation	Improve solutions for low-quality meshes.

3.4. Numerical wind tunnel simulation

As described in Section 3.2, wind tunnel testing is essential for extracting porous media coefficients. However, due to the physical characteristics of trees, conducting such experiments in a wind tunnel is practically unfeasible. Therefore, this study employs a numerical wind tunnel approach to obtain porous media parameters. The CFD tool used for numerical simulations is Simcenter STAR-CCM+ 2310 (Siemens PLM Software, 2023), developed by Siemens. This platform is utilized not only for extracting porous coefficients from the virtual wind tunnel but also for validating subsequent CFD simulations.

The process of numerical wind tunnel simulation proceeds as follows. First, the FBX file of each selected tree is converted into an STL file using the 3D CAD software Rhino 7.0 (McNeel et al., 2023) to enable compatibility with the CFD environment. The converted STL file is imported into Simcenter STAR-CCM+ 2310 as a surface mesh, and the built-in Surface Repair Tool is used to separate the geometry into leaf, branch, and trunk components. Since leaves are modeled as zero-thickness surfaces, they cannot be volumetrically meshed directly; therefore, they are modified to have a uniform thickness of 1 mm.

The numerical wind tunnel duct is designed as a semi-elliptical enclosure that wraps around the tree model, as shown in Fig. 3. The upstream and downstream lengths are set to $5L$ and $10L$, respectively,

where L is the length of the tree (show L in Fig. 3). This ensures fully developed turbulence upstream and prevents wake effects downstream.

Before generating the volume mesh, the Surface Wrapper tool was used to resolve complex surface overlaps between leaves and branches. To preserve the detailed geometry of the foliage and twigs, the base mesh size was set as small as possible. A smaller value for the contact prevention parameter was applied to prevent the merging of overlapping leaf and branch surfaces.

Once the surface wrapping process was completed, a volume mesh was generated using the wrapped surface. A coarser mesh size than that used for the surface wrapper could be applied during this step. Detailed mesh settings are summarized in Table 2, while the resulting volume mesh and cell count for each tree model are presented in Fig. 4. Local mesh refinement was applied to the leaf and branch regions using a wrapper-based approach, to ensure accurate resolution of the tree crown geometry.

The physical models used in the simulation were based on those commonly applied in urban wind environment studies, as summarized in Table 3 (Tominaga et al., 2008). The core framework relies on the Reynolds-Averaged Navier-Stokes (RANS) equations in combination with the realizable $k-\epsilon$ turbulence model, originally developed by Shih et al. (1995). This model has been widely adopted in urban-scale CFD research due to its balanced computational efficiency and ability to accurately capture turbulent kinetic energy and dissipation. Prior studies have validated its applicability in complex urban geometries, particularly in simulating pedestrian-level airflow and ventilation performance (Allegrini and Carmeliet, 2017; Antoniou et al., 2019).

The governing equations of the realizable $k-\epsilon$ turbulence model (Shih et al., 1995) are given below for completeness.

$$\frac{\partial(\rho k)}{\partial t} + \frac{\partial(\rho k u_j)}{\partial x_j} = \frac{\partial}{\partial x_j} \left[\left(\mu + \frac{\mu_t}{\sigma_k} \right) \frac{\partial k}{\partial x_j} \right] + G_k + G_b - \rho \epsilon - Y_M + S_k \quad (5)$$

$$\begin{aligned} \frac{\partial(\rho \epsilon)}{\partial t} + \frac{\partial(\rho \epsilon u_j)}{\partial x_j} = & \frac{\partial}{\partial x_j} \left[\left(\mu + \frac{\mu_t}{\sigma_\epsilon} \right) \frac{\partial \epsilon}{\partial x_j} \right] + \rho C_1 S_\epsilon - \rho C_2 \frac{\epsilon^2}{k + \sqrt{v \epsilon}} + C_{1\epsilon} \frac{\epsilon}{k} C_{3\epsilon} G_b \\ & + S_\epsilon \end{aligned} \quad (6)$$

where, k is the turbulent kinetic energy, ϵ is the dissipation rate, μ_t is the turbulent viscosity, G_k represents the production of turbulent kinetic energy due to mean velocity gradients, and G_b is the production due to buoyancy. Y_M denotes the contribution of fluctuating dilatation in compressible turbulence to the overall dissipation rate. S_k and S_ϵ are user-defined source terms. C_1 , C_2 , $C_{1\epsilon}$, $C_{3\epsilon}$, σ_k and σ_ϵ take standard values as proposed by Shih et al. (1995).

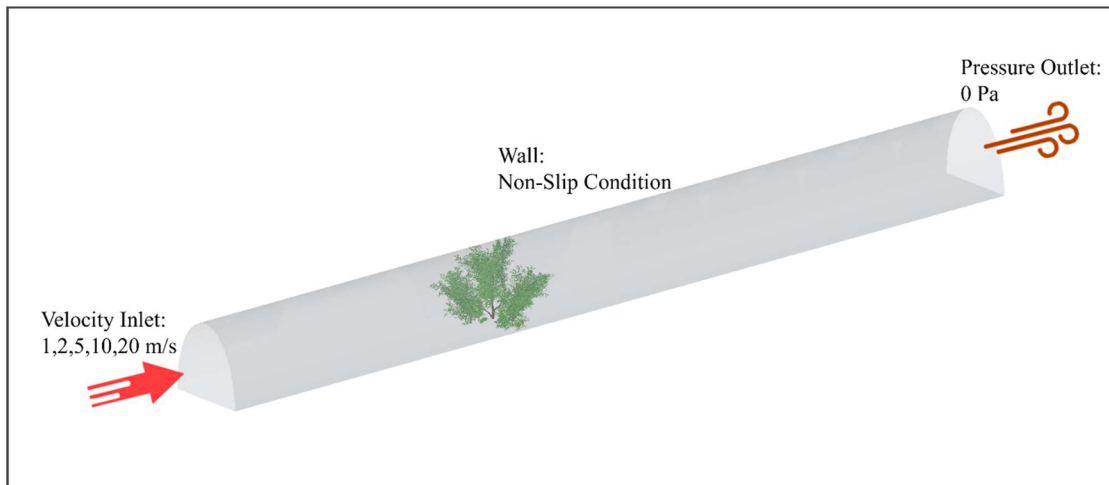


Fig. 5. Numerical wind tunnel geometry and boundary conditions applied in the CFD simulations.

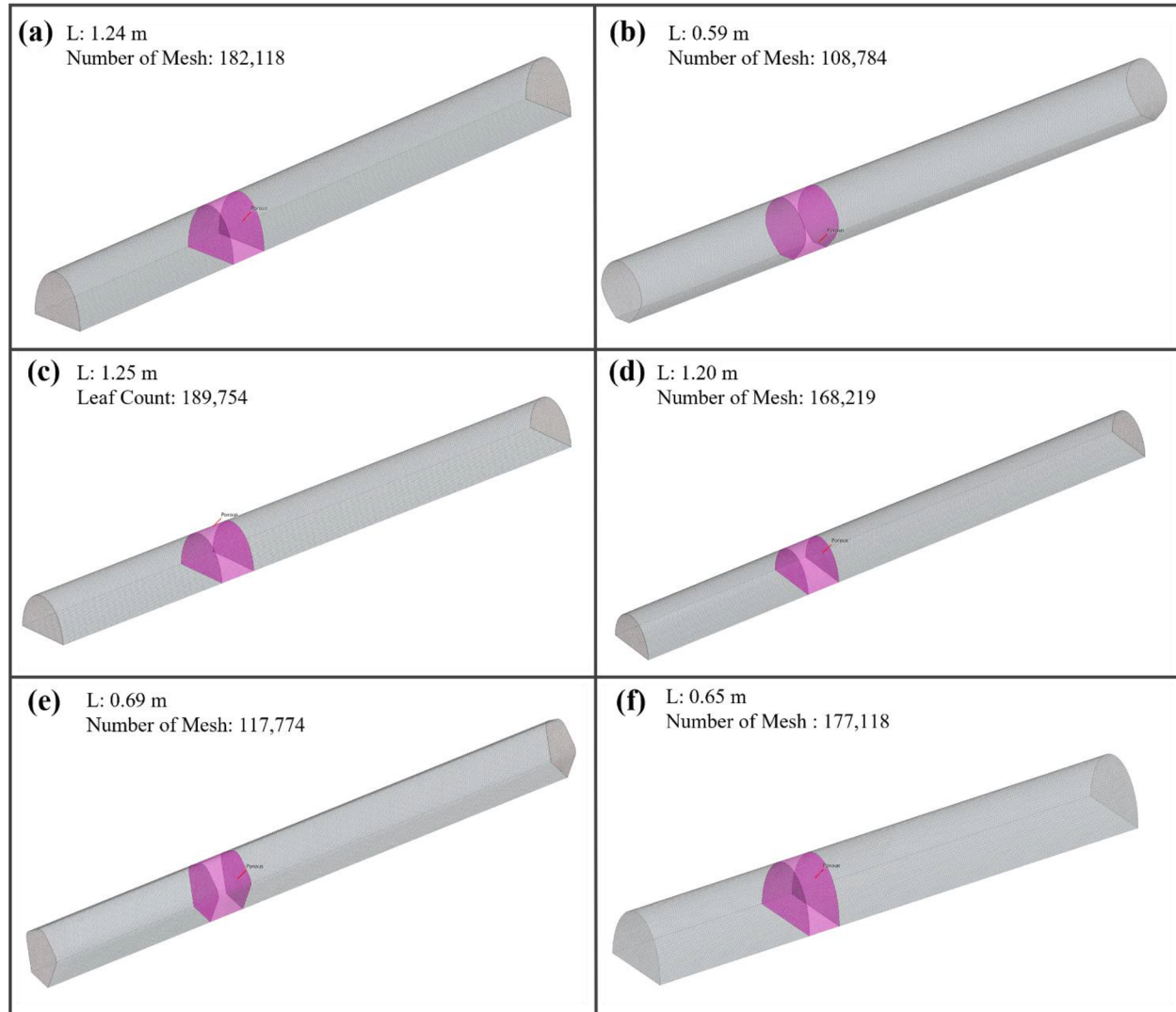


Fig. 6. Numerical wind tunnel geometry and volume mesh for porous resistance validation: (a) *Prunus*, (b) *Ginkgo*, (c) *Chionanthus*, (d) *Zelkova*, (e) *Acer*, (f) *Pinus*.

$$C_1 = \max \left[0.43, \frac{\eta}{\eta + 5} \right], \quad \eta = S \frac{k}{\epsilon}, \quad S = \sqrt{2S_{ij}S_{ij}}$$

These equations have been extensively validated in complex urban geometries, ensuring their suitability for the present simulations.

For the numerical wind tunnel simulations, inlet velocities of 1, 2, 5, 10, and 20 m/s were applied, corresponding to typical wind speed ranges observed in urban environments. This velocity range spans from typical pedestrian-level conditions to stronger gusts and is consistent with values commonly used in prior urban CFD studies (e.g., Tominaga et al., 2008). A fixed pressure outlet boundary condition (0 Pa, gauge) was applied at the downstream end, and no-slip wall conditions were imposed on all duct surfaces to reflect physical wall interactions. The boundary condition configuration is illustrated in Fig. 5.

For each velocity case, the pressure drop across the tree model was computed and normalized by the length of the porous domain (P/L). These data were then used to construct a second-order polynomial fit with a zero intercept, where the coefficients of the quadratic and linear terms were used to determine the inertial resistance (α) and viscous resistance (β), respectively. This procedure was repeated for all selected tree models to extract their corresponding porous media parameters.

To validate the extracted porous resistance values, the same wind tunnel geometry was used, with the central tree domain replaced by a porous region equivalent to the actual tree length. The geometry and

mesh configurations for each tunnel are shown in Fig. 6. A base mesh size of 0.05 m was applied, and very thin prism layers (absolute thickness of 0.001 m) were used to ensure that wall y_+ values remained below 1 across all velocity conditions. The computed resistance coefficients (α and β) were then implemented as porous media properties. Although the dominant flow is expected to be streamwise, tree resistance was assumed to be isotropic; hence, the same values were applied in the X, Y, and Z directions. As in the parameter extraction stage, simulations were conducted with inlet velocities of 1, 2, 5, 10, and 20 m/s. The resulting pressure drops were compared with the original simulation results to validate the porous resistance parameters.

To validate the extracted porous resistance values, the same wind tunnel geometry was used, with the central tree domain replaced by a porous region equivalent to the actual tree length. The geometry and mesh configurations for each tunnel are shown in Fig. 6. A base mesh size of 0.05 m was applied, and very thin prism layers (absolute thickness of 0.001 m) were used to ensure that wall y_+ values remained below 1 across all velocity conditions. The computed resistance coefficients (α and β) were then implemented as porous media properties. Although the dominant flow is expected to be streamwise, tree resistance was assumed to be isotropic; hence, the same values were applied in the X, Y, and Z directions. As in the parameter extraction stage, simulations were conducted with inlet velocities of 1, 2, 5, 10, and 20 m/s. The resulting pressure drops were compared with the original

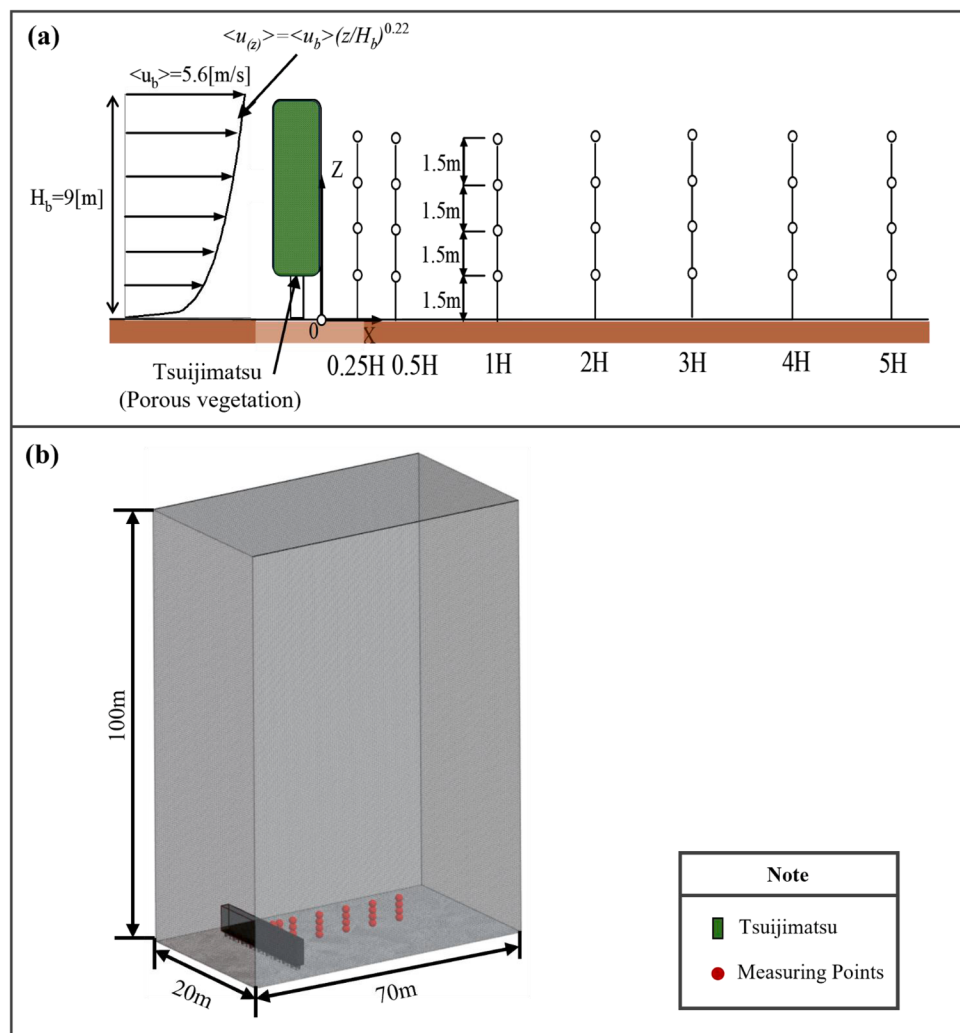


Fig. 7. Schematic of the reference wind tunnel setup and corresponding CFD domain used for validation. (a) Experimental configuration adapted from Iwata et al. (2003). (b) CFD model with porous vegetation and probe locations.

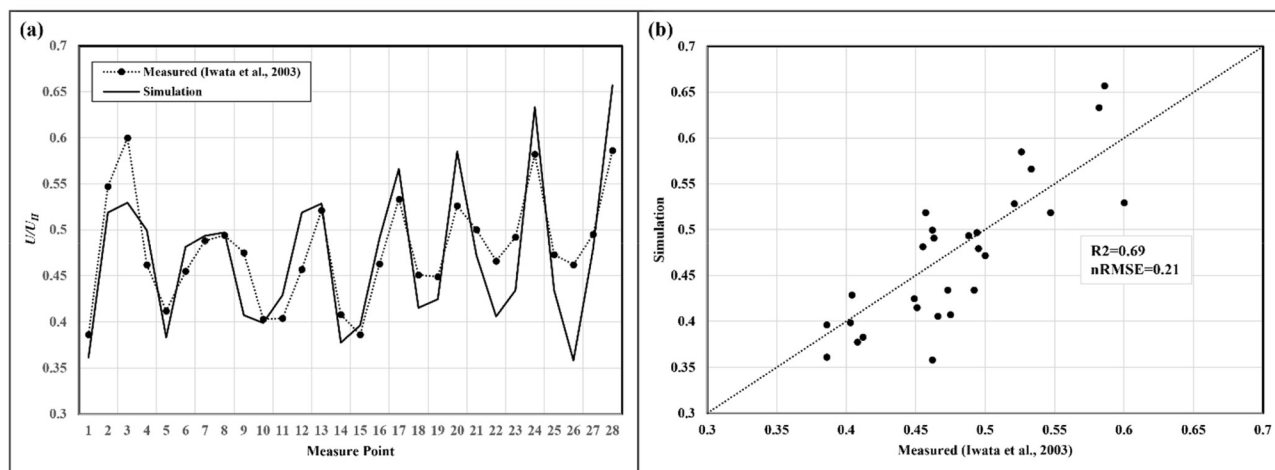


Fig. 8. Validation results for *Pinus thunbergii* using CFD-based porous media simulation.

(a) Comparison of normalized velocity ratios ($U//U_H$) between measurements and simulation across 28 probe locations. (b) Correlation between measured and simulated velocities; the dotted line indicates the 1:1 reference line.

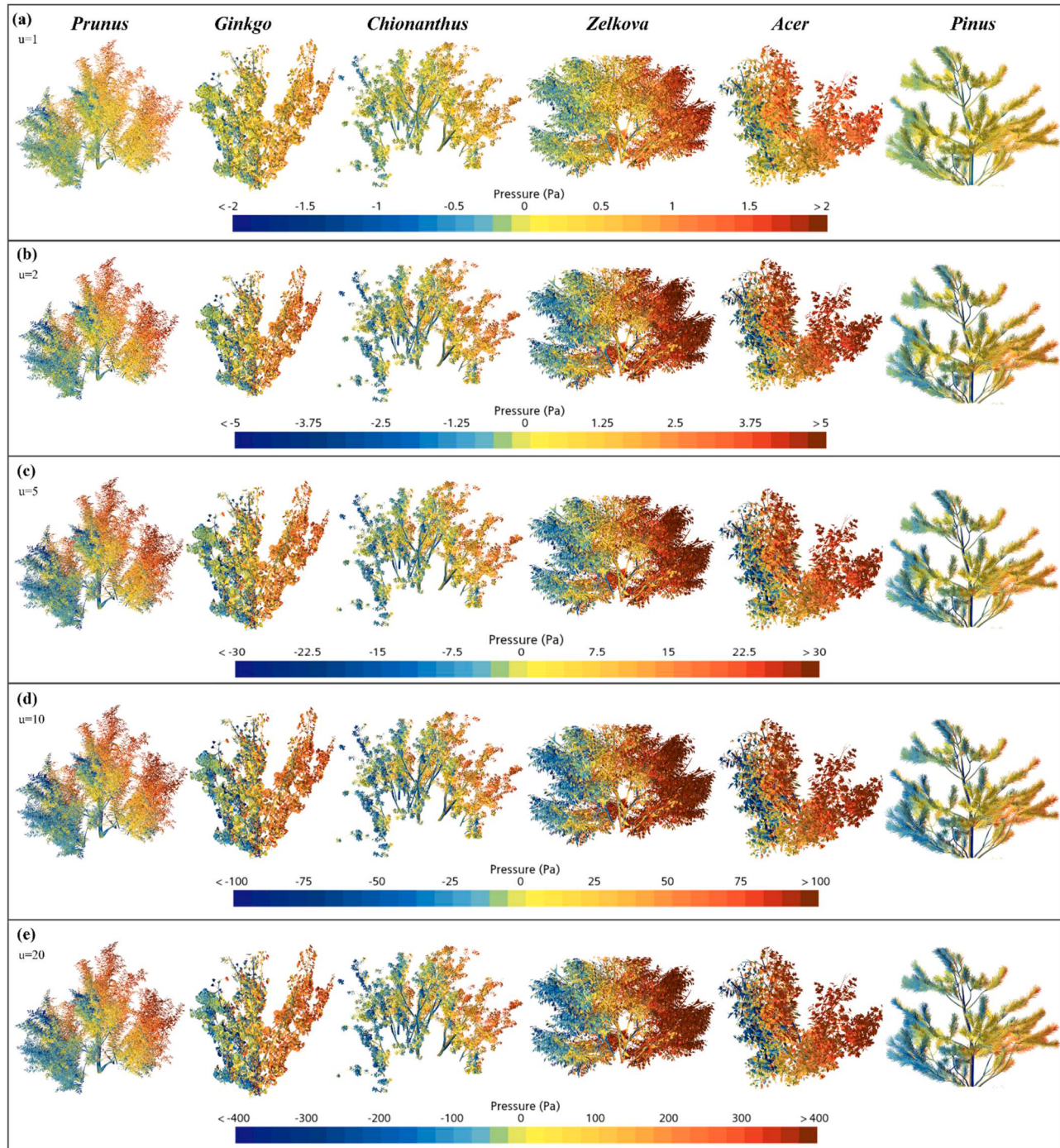


Fig. 9. Pressure distributions around the tree model under varying inlet wind speeds: (a) $U = 1 \text{ m/s}$, (b) $U = 2 \text{ m/s}$, (c) $U = 5 \text{ m/s}$, (d) $U = 10 \text{ m/s}$, (e) $U = 20 \text{ m/s}$.

simulation results to validate the porous resistance parameters.

3.5. Validation

To validate the numerical wind tunnel, a comparative analysis was conducted using experimental data from Iwata et al. (2003), which measured wind speed reduction behind a Japanese pine windbreak (*Tsujimatsu*). The tree species used in the reference study, *Pinus thunbergii*, is identical to the species for which 3D geometry data is available in this study, allowing for a direct simulation under comparable conditions. The experimental configuration and measurement locations are illustrated in Fig. 7(a). Wind speeds were measured at seven downstream positions ($0.25H, 0.5H, 1.0H, 2H, 3H, 4H$, and $5H$), with four

vertical probes placed at 1.5 m intervals at each location.

The CFD domain for validation was constructed with dimensions of 70 m in length and 100 m in height, following the setup proposed in the reference. As the original study employed a 2D simulation, the domain width was set to 20 m based on photographic analysis of the windbreak. The 3D CFD domain configuration, porous vegetation region, and probe locations are shown in Fig. 7(b). The total number of mesh cells used in the simulation was 5110,846. The same physical models as those in the numerical wind tunnel were applied, and the inlet velocity boundary condition followed the vertical wind profile proposed in the reference study.

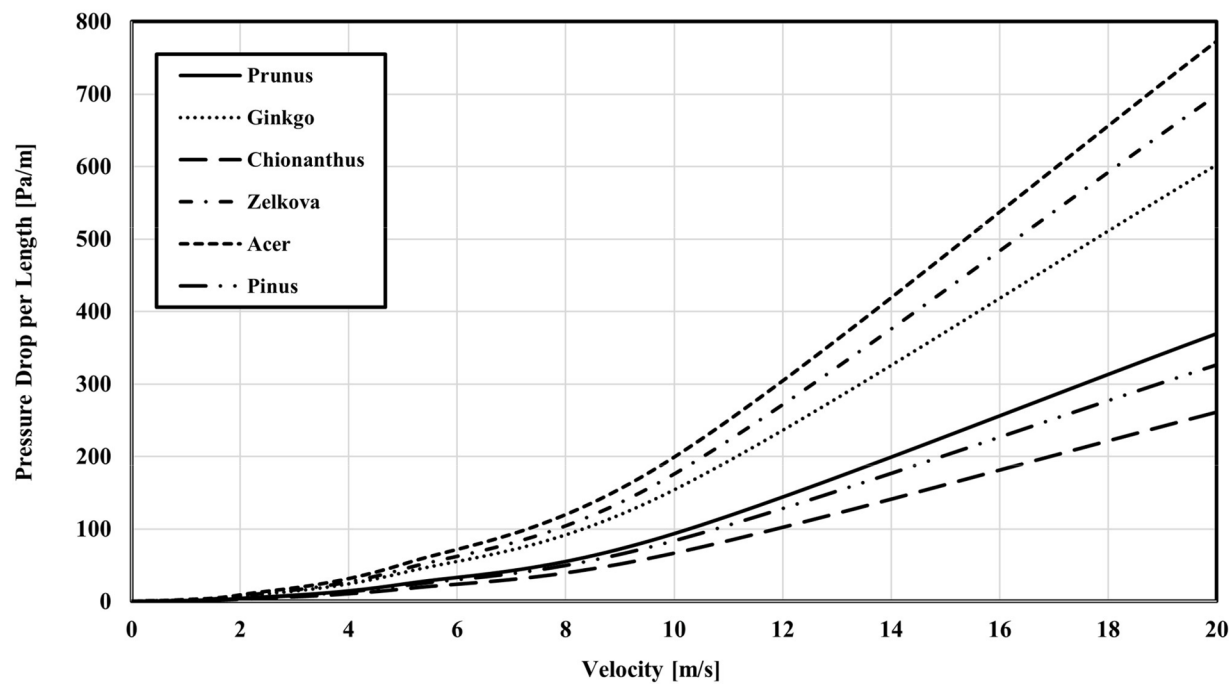


Fig. 10. Pressure–velocity relationships used to derive porous resistance coefficients for six major street tree species. Second-order polynomial fitting curves were used for resistance parameter extraction.

Table 4

Extracted porous resistance coefficients (α : inertial resistance, β : viscous resistance) for six major street tree species.

Tree species	Inertial resistance (α) [kg/m^4]	Viscous resistance (β) [$\text{kg}/\text{m}^3 \cdot \text{s}$]
<i>Prunus</i>	0.91497	0.17433
<i>Ginkgo</i>	1.47814	0.55017
<i>Chionanthus</i>	0.64302	0.19590
<i>Zelkova</i>	1.73656	0.18038
<i>Acer</i>	1.88413	0.94812
<i>Pinus</i>	0.79962	0.33728

$$u_z = u_b \cdot \left(\frac{z}{H_b} \right)^{0.22} \quad (3a)$$

Unlike the parameter extraction stage, where constant inlet velocities (1, 2, 5, 10, and 20 m/s) were applied to provide a uniform basis for comparing aerodynamic resistance across different tree species, the validation stage adopted a vertical wind profile to reproduce realistic urban wind conditions. This distinction is important because tree heights vary among species, making profile-based extraction inconsistent, whereas constant velocities allow systematic derivation of porous coefficients. Validation with a wind profile, on the other hand, ensures comparability with field measurements of *Pinus thunbergii* windbreaks.

Here, u_z denotes the inlet velocity profile as a function of height, with $u_b = 5.56$ m/s representing the velocity at tree height $H_b = 9$ m, and z denoting height. Guidelines were also provided for the initial and inlet turbulence parameters: the turbulent kinetic energy was set to $k = 3.02$ J/kg, and the turbulent dissipation rate was set to $\varepsilon = 0.6 \text{ m}^2/\text{s}^3$.

The validation simulation results showed reasonable agreement with the measured data, yielding a R^2 of 0.69 and a normalized root mean square error (nRMSE) of 21 %. These results suggest that the porous media parameters extracted from the numerical wind tunnel approach are physically meaningful. A detailed comparison is presented in Section 4.1.

Table 5

Comparison of pressure drops from real tree and porous models for six street tree species at inlet velocities of 1–20 m/s.

Tree Species	Velocity [m/s]	P/L [Pa/m]	Pressure [Pa]		Error [%]
			Tree	Porous	
<i>Prunus</i>	1	1.02	1.26	1.48	15.03
	2	3.90	4.84	5.38	10.13
	5	23.67	29.35	31.41	6.54
	10	93.35	115.75	121.98	5.10
	20	369.45	458.12	479.27	4.41
<i>Ginkgo</i>	1	1.72	1.03	1.41	27.05
	2	6.57	3.91	4.74	17.55
	5	39.40	23.46	26.56	11.68
	10	153.76	91.54	98.46	7.02
	20	602.17	358.52	377.95	5.14
<i>Chionanthus</i>	1	0.74	0.93	1.21	23.62
	2	2.83	3.54	4.19	15.68
	5	16.97	21.24	23.21	8.47
	10	66.40	83.14	89.15	6.74
	20	261.10	326.95	347.70	5.96
<i>Zelkova</i>	1	1.83	2.20	2.56	14.01
	2	7.20	8.67	9.50	8.75
	5	44.23	53.27	56.67	5.99
	10	175.58	211.46	222.44	4.93
	20	698.21	840.90	880.47	4.49
<i>Acer</i>	1	2.39	1.64	2.40	31.74
	2	8.80	6.04	7.76	22.21
	5	51.11	35.05	39.97	12.29
	10	198.76	136.33	146.16	6.73
	20	772.45	529.84	556.64	4.81
<i>Pinus</i>	1	0.98	0.68	0.855	25.680
	2	3.63	2.48	2.899	16.780
	5	21.51	14.08	15.326	8.860
	10	83.57	54.83	57.937	5.670
	20	326.52	212.91	222.507	4.510

4. Results and discussion

4.1. Validation against reference data

To evaluate the reliability of the porous media parameters extracted

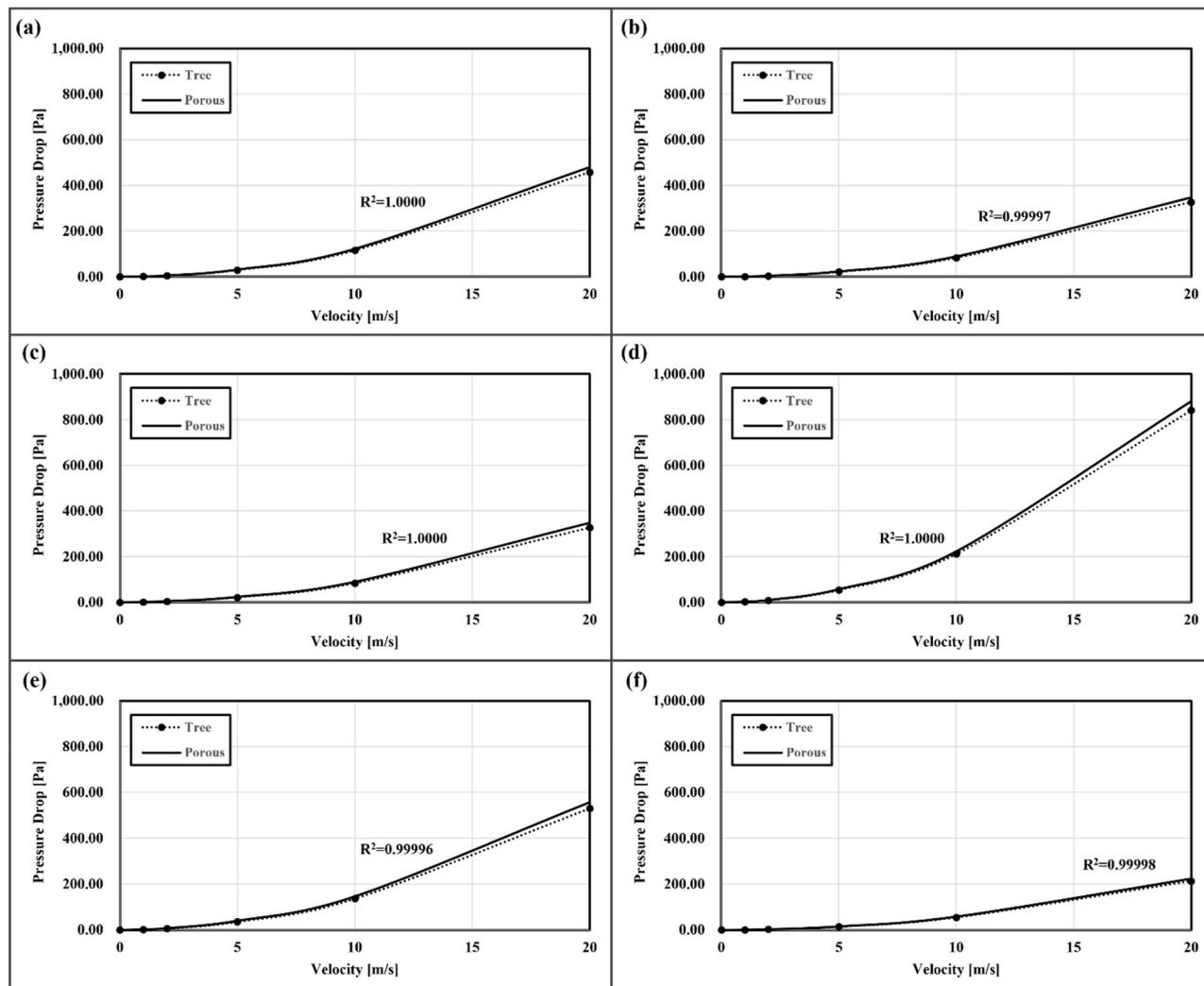


Fig. 11. Comparison of pressure drop trends between the detailed tree model and the porous model for six street tree species: (a) *Prunus*, (b) *Ginkgo*, (c) *Chionanthus*, (d) *Zelkova*, (e) *Acer*, (f) *Pinus*.

Table 6
Leaf structural traits and corresponding resistance coefficients of six tree species.

Tree species	L [mm]	Number of leaves [EA]	Average leaf area [mm^2]	Leaf volume fraction [%]	α [kg/m^4]	β [$\text{kg}/\text{m}^3 \cdot \text{s}$]
<i>Prunus</i>	1242	9312	1263.75	6.00	0.91497	0.17433
<i>Ginkgo</i>	595	3486	1417.23	5.99	1.47814	0.55017
<i>Chionanthus</i>	1252	18,080	367.78	2.68	0.64302	0.19590
<i>Zelkova</i>	1204	6193	2741.48	6.34	1.73656	0.18038
<i>Acer</i>	686	2122	1120.45	6.97	1.88413	0.94812
<i>Pinus</i>	652	20,967	545.51	2.76	0.79962	0.33728

through the numerical wind tunnel procedure, simulation results were compared with wind tunnel measurements for *Pinus thunbergii* reported by Iwata et al. (2003).

Fig. 8(a) shows the normalized velocity ratios at each of the 28 probe locations positioned downstream of the tree model. The simulation reproduced the overall trend of wake flow reduction, particularly in the mid-wake region ($1H$ to $3H$), where the flow begins to recover. In the near-wake region ($0.25H$ to $1H$), however, the simulation tended to slightly underestimate the measured velocities, while in the far-wake region ($4H$ to $5H$), the fluctuations in both measured and simulated values became more pronounced. These localized discrepancies may result from the simplification of tree geometry into a uniform porous zone, as well as the assumption of isotropic aerodynamic resistance

across all directions.

A statistical comparison between the measured and simulated data is presented in Fig. 8(b). The results showed a R^2 of 0.69 and a nRMSE of 21 %. Although these values fall short of high-precision thresholds, they are considered reasonable given the limitations of the modeling approach. Specifically, the use of single-scale, isotropic porous representation inherently neglects directional and structural complexities of real vegetation, such as canopy porosity variation and asymmetry.

To further examine the spatial characteristics of the model's accuracy, the wake region was subdivided into three zones—near (0 – $1H$), mid (1 – $3H$), and far (3 – $5H$)—and validation statistics were evaluated separately for each. The mid-wake region exhibited the best agreement, with $R^2 = 0.727$ and nRMSE = 0.259, indicating that the extracted

porous coefficients effectively capture the core aerodynamic behavior. In the near-wake, R^2 was 0.612 and nRMSE was 0.183, suggesting slight underprediction due to enhanced drag effects from the simplified model. The far-wake region showed high correlation ($R^2 = 0.910$) but elevated error (nRMSE = 0.391), reflecting accumulated deviations and flow variability in the downstream field.

While the far-wake region exhibited the largest fluctuations, this zone is generally of limited practical importance in urban CFD applications, which typically focus on near-field flow behavior around buildings and vegetation.

Overall, the model successfully captured the general aerodynamic response of the tree and reproduced the spatial distribution of wind speed reduction with acceptable accuracy. This indicates that the porous resistance parameters extracted through the proposed CFD-based method are physically valid and practically applicable to simplified vegetation modeling in urban-scale simulations.

4.2. Extraction of porous resistance parameters

Based on the validated method presented in Section 4.1, porous resistance parameters for six major street tree species were extracted using numerical wind tunnel simulations. Pressure drop simulations were conducted for each species under inlet velocities commonly observed in urban environments ($U = 1, 2, 5, 10$, and 20 m/s).

As shown in Fig. 9, the pressure drop increases with inlet velocity, and a more distinct pressure gradient is observed across the tree crown. This demonstrates the enhanced aerodynamic drag induced by the vegetation structure. In addition, noticeable differences in pressure distribution under the same velocity conditions across species indicate that aerodynamic resistance varies depending on the tree type.

To quantify this resistance, the pressure–velocity relationships were fitted using second-order polynomials, as described in Section 3.2. The derived curves are presented in Fig. 10, which served as the basis for extracting the porous resistance coefficients.

Each species exhibited a unique fitting trend depending on its leaf structure, and all curves showed excellent agreement ($R^2 \approx 1.00$), confirming the consistency of the simulation results across species.

The resulting coefficients— α (inertial resistance) and β (viscous resistance)—are summarized in Table 4 and subsequently applied in the porous model validation in Section 4.3.

4.3. Validation of porous resistance parameters

To verify the accuracy of the porous resistance coefficients extracted from the numerical wind tunnel simulations, an additional simulation was conducted using a porous model. For each tree species, a porous region of length L was defined in the same wind tunnel domain, and the corresponding resistance coefficients were applied uniformly in all directions. The resulting pressure drops were then compared to the original numerical wind tunnel simulations and are summarized in Table 5.

In the pressure data, the Tree values refer to the results from the detailed numerical tree model, whereas the porous values correspond to those from the porous model validation. At low velocities, the absolute pressure difference between the two models is small, resulting in seemingly large percentage errors. However, this is a typical characteristic of percentage-based error metrics and does not indicate poor model performance. Conversely, at higher pressure regions, the error remains within approximately 5 %, indicating that the resistance coefficients accurately reproduce the aerodynamic behavior of the tree model. This slight overestimation in pressure drop implies that urban-scale simulations using porous parameters may result in a more conservative assessment of vegetation-induced aerodynamic resistance.

To further illustrate this agreement, Fig. 11 presents pressure–velocity relationships for all six species, comparing the results from the tree model and the porous model. The two curves show a consistently high degree of overlap across the velocity range, and the fitted

data exhibit exceptionally strong correlation values ($R^2 \approx 0.9999$ for all species).

This high correlation is expected given the smooth and monotonic pressure–velocity trends under controlled wind tunnel simulation conditions. Moreover, minor deviations observed between the fitted and simulated curves indicate that the results are physically meaningful and not simply overfitted.

These results demonstrate that the porous resistance coefficients can reliably reproduce the aerodynamic effects of complex tree structures without requiring detailed geometric modeling. This significantly reduces modeling complexity and computational cost while maintaining high simulation fidelity across various species.

4.4. Interpretation of resistance characteristics by species

To investigate the physical meaning of the extracted porous resistance parameters, the geometric characteristics of each tree species were analyzed in terms of leaf count, average leaf area, and volumetric leaf density (leaf volume fraction). Table 6 summarizes these canopy traits along with the corresponding resistance coefficients (α, β), enabling a comparative interpretation between physical leaf structure and aerodynamic resistance.

The volumetric leaf density was relatively consistent across species, ranging from approximately 6 % to 7 %, suggesting similar overall porosity levels. However, distinct variations in resistance were observed depending on leaf morphology and distribution.

Despite having a relatively low volumetric density, *Ginkgo* and *Acer* exhibited the highest resistance coefficients. This can be attributed to their broad, flat leaf shapes, which increase frontal area and aerodynamic drag. In contrast, *Zelkova* — which had the largest average leaf area — showed a comparatively low resistance value, likely due to its elongated and sparse leaf structure that allows greater airflow penetration. *Prunus* also exhibited low resistance, consistent with its narrow leaf shape. On the other hand, *Chionanthus* and *Pinus* had both small leaf areas and low volumetric densities, resulting in the lowest resistance values.

These results suggest that porous resistance is not solely determined by leaf quantity or density, but is strongly influenced by the effective aerodynamic blockage, which depends on both leaf morphology and spatial arrangement.

4.5. Discussion and study limitation

The porous resistance parameters extracted for six major street tree species revealed considerable variability depending on morphological characteristics. For example, *Acer* and *Ginkgo* exhibited the highest inertial resistance values (α), which can be attributed to their large total leaf area and relatively broad, flat leaf shapes. Conversely, *Chionanthus* and *Pinus* showed lower α values, likely due to their small leaf area or needle-like foliage, resulting in less frontal blockage against airflow.

Interestingly, *Zelkova*, despite having the largest average leaf area, demonstrated relatively moderate aerodynamic resistance. This can be explained by its narrow leaf geometry, which reduces drag despite its surface area. Similarly, *Prunus*, which has a dense but elongated leaf structure, also exhibited moderate resistance values.

These findings suggest that aerodynamic resistance is not solely dependent on leaf area or density, but is significantly influenced by leaf shape, orientation, and spatial arrangement. This supports the importance of species-specific calibration when applying porous models in urban CFD simulations. This relationship is summarized in Table 6, which presents resistance parameters alongside representative morphological traits for each species. These results highlight the potential of using porous coefficients to simplify urban vegetation modeling, particularly in large-scale or long-term simulations where geometric detail is computationally prohibitive.

The validated porous coefficients can greatly simplify urban

vegetation modeling by replacing detailed tree geometries with representative porous zones. This is particularly beneficial for large-scale or long-term simulations, where geometric complexity and meshing requirements can become computationally prohibitive.

However, some limitations remain. The model does not account for seasonal variability in foliage (e.g., leaf shedding), wind-induced leaf motion, or thermal interactions, which may influence aerodynamic behavior under real conditions. Future work should aim to incorporate dynamic vegetation properties and also evaluate thermal performance under varying meteorological scenarios.

Overall, the proposed porous model demonstrates high potential for practical application in urban wind and ventilation studies, offering a balance between computational efficiency and physical realism when species-specific resistance values are applied.

5. Conclusion

This study proposed a CFD-based methodology for extracting and validating porous resistance parameters for six major street tree species commonly found in urban environments. By replacing complex tree geometries with porous media, the study aimed to simplify vegetation modeling while maintaining aerodynamic fidelity. Using numerical wind tunnel simulations, porous resistance values were derived through pressure–velocity curve fitting, and their accuracy was verified through comparison with full-scale tree models.

The key conclusions of this study are as follows:

- The extracted porous resistance coefficients (α , β) showed species-specific variation closely related to leaf morphology and structure, demonstrating that aerodynamic resistance is strongly influenced by leaf shape, orientation, and spatial arrangement rather than leaf volume alone.
- The porous models accurately reproduced pressure drops patterns observed in full-scale tree models, with errors below 5 % at higher velocities and exceptionally high correlations ($R^2 \approx 0.9999$), confirming the validity of the proposed approach.
- The validated porous coefficients can effectively replace detailed geometric tree modeling in CFD simulations, offering significant reductions in modeling complexity and computational cost, particularly in large-scale urban analyses. Moreover, their application enables more accurate representation of vegetation-induced aerodynamic effects in urban environmental simulations, thereby enhancing the overall fidelity of the modeled thermal and wind environments.

This study confirms that a porous media approach based on species-specific resistance values can serve as a practical alternative to complex vegetation modeling in CFD. The method allows for the reliable representation of aerodynamic behavior across various species and environmental conditions, thereby facilitating efficient urban wind flow simulations and climate analysis.

These findings provide a useful framework for urban microclimate modeling, supporting the development of vegetation-informed design strategies and enabling more efficient thermal and ventilation planning in urban environments. These applications include urban ventilation analysis, pollution dispersion modeling, and green infrastructure planning. This approach can be readily incorporated into real-world urban planning processes and large-scale environmental simulations to support data-informed design decisions.

Declaration of generative AI and AI-assisted technologies in the writing process

During the preparation of this work, the author used ChatGPT to improve the clarity and readability of some sentences. After using this tool, the author reviewed and edited the content as needed and take full

responsibility for the content of the publication.

CRediT authorship contribution statement

Junghyeon Ahn: Writing – review & editing, Writing – original draft, Visualization, Validation, Software, Methodology, Investigation, Formal analysis, Data curation, Conceptualization. **Junsuk Kang:** Writing – review & editing, Writing – original draft, Supervision, Software, Resources, Project administration, Methodology, Funding acquisition, Conceptualization.

Declaration of competing interest

The authors declare that they have no known competing financial interests or personal relationships that could have appeared to influence the work reported in this paper.

Acknowledgement

This work was supported by knowledge-based environmental service program and Korea Environment Industry & Technology Institute (KEITI) through Climate Change R&D Project for New Climate Regime, funded by the Korea Ministry of Environment (MOE) (2022003570004), and the National Research Foundation of Korea Grant funded by the Korean Government (NRF-RS-2023-00259403).

Data availability

Data will be made available on request.

Data availability

Data will be made available on request.

References

- Ahn, J., Kim, J., Kang, J., 2025. Development of an artificial intelligence model for CFD data augmentation and improvement of thermal environment in urban areas using nature-based solutions. *Urban. For. Urban. Green.* 104, 128629. <https://doi.org/10.1016/j.ufug.2024.128629>.
- Allegrini, J., Carmeliet, J., 2017. Coupled CFD and building energy simulations for studying the impacts of building height topology and buoyancy on local urban microclimates. *Urban. Clim.* 21, 278–305. <https://doi.org/10.1016/j.ulcim.2017.07.005>.
- Amani-Beni, M., Tabatabaei Malazi, M., Dehghanian, K., Akbari, H., 2023. Investigating the effects of wind loading on three-dimensional tree models using numerical simulation with implications for urban design. *Sci. Rep.* 13, 7277. <https://doi.org/10.1038/s41598-023-34071-5>.
- Amorim, J.H., Rodrigues, V., Tavares, R., Valente, J., Borrego, C., 2013. CFD modelling of the aerodynamic effect of trees on urban air pollution dispersion. *Sci. Total. Environ.* 461, 541–551. <https://doi.org/10.1016/j.scitotenv.2013.05.031>.
- Antoniou, N., Montazeri, H., Neophytou, M., Blocken, B., 2019. CFD simulation of urban microclimate: validation using high-resolution field measurements. *Sci. Total Env.* 695, 133743. <https://doi.org/10.1016/j.scitotenv.2019.133743>.
- Baek, S., Kim, J., Kang, J., 2024. Impact of green infrastructure on PM10 in port-adjacent residential complexes: a finite volume method-based computational fluid dynamics study. *Sustain. Cities. Soc.* 115, 105815. <https://doi.org/10.1016/j.scs.2024.105815>.
- Buccolieri, R., Sandberg, M., Di Sabatino, S., 2010. City breathability and its link to pollutant concentration distribution within urban-like geometries. *Atmos. Env.* 44 (15), 1894–1903. <https://doi.org/10.1016/j.atmosenv.2010.02.022>.
- Cao, J., Tamura, Y., Yoshida, A., 2012. Wind tunnel study on aerodynamic characteristics of shrubby specimens of three tree species. *Urban. For. Urban. Green.* 11 (4), 465–476. <https://doi.org/10.1016/j.ufug.2012.05.003>.
- Darcy, H. (1856). Les fontaines publiques de la ville de Dijon: exposition et application des principes à suivre et des formules à employer dans les questions de distribution d'eau: ouvrage terminé par un appendice relatif aux fournitures d'eau de plusieurs villes, au filtrage des eaux et à la fabrication des tuyaux de fonte, de plomb, de tôle et de bitume (Vol. 2). Victor Dalmont, éditeur.
- De Langre, E., 2008. Effects of wind on plants. *Annu. Rev. Fluid. Mech.* 40, 141–168. <https://doi.org/10.1146/annurev.fluid.40.111406.102135>.
- Escobedo, F.J., Kroeger, T., Wagner, J.E., 2011. Urban forests and pollution mitigation: analyzing ecosystem services and disservices. *Environ. Pollut.* 159 (8–9), 2078–2087. <https://doi.org/10.1016/j.envpol.2011.01.010>.

- Forchheimer, P., 1901. Wasserbewegung Durch Boden. *Zeitschrift des Vereines Deutscher Ingenieuer*.
- Grimmond, C.S.B., Oke, T.R., 1999. Aerodynamic properties of urban areas derived from analysis of surface form. *J. Appl. Meteorol.* 38 (9), 1262–1292. [https://doi.org/10.1175/1520-0450\(1999\)038<1262:APOUAD>2.0.CO;2](https://doi.org/10.1175/1520-0450(1999)038<1262:APOUAD>2.0.CO;2).
- Gromke, C., Ruck, B., 2007. Influence of trees on the dispersion of pollutants in an urban street canyon—Experimental investigation of the flow and concentration field. *Atmos. Env.* 41 (16), 3287–3302. <https://doi.org/10.1016/j.atmosenv.2006.12.043>.
- Gromke, C., Ruck, B., 2008. Aerodynamic modelling of trees for small-scale wind tunnel studies. *Forestry* 81 (3), 243–258. <https://doi.org/10.1093/forestry/cpn018>.
- Gromke, C., Ruck, B., 2009. On the impact of trees on dispersion processes of traffic emissions in street canyons. *Bound. Layer Meteorol.* 131 (1), 19–34. <https://doi.org/10.1007/s10546-008-9300-2>.
- Hong, S.W., Zhao, L., Zhu, H., 2018. CFD simulation of airflow inside tree canopies discharged from air-assisted sprayers. *Comput. Electron. Agric.* 149, 121–132. <https://doi.org/10.1016/j.compag.2018.04.014>.
- Iwata, T., Kimura, A., Mochida, A., Yoshino, H., Ooka, R., Yoshida, S., 2003. Numerical analysis of windbreak effect on velocity reduction based on plant canopy model. *Summaries of Technical Papers of Annual Meeting of the Architectural Institute of Japan (D-2)*, pp. 745–746 (in Japanese).
- Kim, J., Kang, J., 2023. AI-based temperature reduction effect model of fog cooling for human thermal comfort: climate adaptation technology. *Sustain. Cities. Soc.* 95, 104574. <https://doi.org/10.1016/j.scs.2023.104574>.
- Korea Forest Service, 2022. 2020 National Street Tree Statistics [Data File]. Korea Forest Service Open Data Portal. [https://www.forest.go.kr/kfswb/cop/bbs/selectBoardArticle.do?jsessionid=glZjaMAFDBx1YjBBZY3DsZdBITKDXJ4NSWUvqiU1uvTkpx7R8tzPnyfRAsJhxY.frswas02_servet_engine5?nttId=3168675&bbsId=BBSMSTR_1069&pageIndex=1&pageUnit=10&searchtitle=title&searchcontent=&searchkey=&searchwriter=&searchdept=&searchWrd=&ctgryLrcs=CTGRY159&ctgryMdcls=&ctgrySmcls=&ntcStartDt=&ntcEndDt=&orgId=&mnn=NKF_S.06.09.01&component="](https://www.forest.go.kr/kfswb/cop/bbs/selectBoardArticle.do?jsessionid=glZjaMAFDBx1YjBBZY3DsZdBITKDXJ4NSWUvqiU1uvTkpx7R8tzPnyfRAsJhxY.frswas02_servet_engine5?nttId=3168675&bbsId=BBSMSTR_1069&pageIndex=1&pageUnit=10&searchtitle=title&searchcontent=&searchkey=&searchwriter=&searchdept=&searchWrd=&ctgryLrcs=CTGRY159&ctgryMdcls=&ctgrySmcls=&ntcStartDt=&ntcEndDt=&orgId=&mnn=NKF_S.06.09.01&component=)
- Liu, C., Zheng, Z., Cheng, H., Zou, X., 2018. Airflow around single and multiple plants. *Agric Meteorol* 252, 27–38. <https://doi.org/10.1016/j.agrmet.2018.01.009>.
- Manickathan, L., Defraeye, T., Allegrini, J., Derome, D., Carmeliet, J., 2018a. Comparative study of flow field and drag coefficient of model and small natural trees in a wind tunnel. *Urban. For. Urban. Green.* 35, 230–239. <https://doi.org/10.1016/j.ufug.2018.09.011>.
- Manickathan, L., Defraeye, T., Allegrini, J., Derome, D., Carmeliet, J. (2018). Parametric study of the influence of environmental factors and tree properties on the transpirative cooling effect of trees. *Agricul. Forest Meteorol.*, 248, 259–274. <https://doi.org/10.3929/ethz-b-000198634>.
- McNeel, R., et al., 2023. Rhino – New in Rhino 7. <https://www.rhino3d.com/7/new>.
- McPherson, E.G., Nowak, D.J., Rowntree, R.A., 1994. Chicago's Urban Forest Ecosystem: Results of the Chicago Urban Forest Climate Project.
- Milliez, M., Carissimo, B., 2007. Numerical simulations of pollutant dispersion in an idealized urban area, for different meteorological conditions. *Bound. Layer Meteorol.* 122 (2), 321–342. <https://doi.org/10.1007/s10546-006-9109-4>.
- Ministry of Science and ICT, 2023. 3D Growth Data of Urban Trees [Data Set]. AI Hub. <https://www.aihub.or.kr/aihubdata/data/view.do?dataSetSn=71458>.
- Moonen, P., Defraeye, T., Dorer, V., Blocken, B., Carmeliet, J., 2012. Urban physics: effect of the micro-climate on comfort, health and energy demand. *Front. Archit. Res.* 1 (3), 197–228. <https://doi.org/10.1016/j foar.2012.05.002>.
- Nowak, D.J., Crane, D.E., Stevens, J.C., 2006. Air pollution removal by urban trees and shrubs in the United States. *Urban. For. Urban. Green.* 4 (3–4), 115–123. <https://doi.org/10.1016/j.ufug.2006.01.007>.
- Ren, X., Zhang, G., Chen, Z., Zhu, J., 2023. The influence of wind-induced response in urban trees on the surrounding flow field. *Atmosphere* 14 (6), 1010. <https://doi.org/10.3390/atmos14061010>.
- Rudnicki, M., Mitchell, S.J., Novak, M.D., 2004. Wind tunnel measurements of crown streamlining and drag relationships for three conifer species. *Can. J. For. Res.* 34 (3), 666–676. <https://doi.org/10.1139/x03-233>.
- Santiago, J.L., Martín, F., Martín, F., 2007. CFD simulation of airflow over a regular array of cubes. Part I: three-dimensional simulation of the flow and validation with wind tunnel measurements. *Bound. Layer Meteorol.* 122 (3), 609–634. <https://doi.org/10.1007/s10546-006-9124-7>.
- Shih, T.-H., Liou, W.W., Shabbir, A., Yang, Z., Zhu, J., 1995. A new k- ϵ eddy viscosity model for high Reynolds number turbulent flows. *Comput. Fluids.* 24, 227–238. [https://doi.org/10.1016/0045-7930\(94\)00032-T](https://doi.org/10.1016/0045-7930(94)00032-T).
- Siemens PLM Software, 2023. Simcenter STAR-CCM+ 2310 user guide.
- Sogachev, A., Panferov, O., 2006. Modification of two-equation models to account for plant drag. *Bound. Layer Meteorol.* 121 (2), 229–266. <https://doi.org/10.1007/s10546-006-9073-5>.
- Tominaga, Y., Mochida, A., Yoshie, R., Kataoka, H., Harimoto, K., Nozu, T., 2008. AJI guidelines for practical applications of CFD to pedestrian wind environment around buildings. *J. Wind Eng. Ind. Aerodyn.* 96 (10–11), 1749–1761. <https://doi.org/10.1016/j.jweia.2008.02.058>.
- Zhang, C., Zhou, H., Xu, L., Ru, Y., Ju, H., Chen, Q., 2022. Wind tunnel study of the changes in drag and morphology of three fruit tree species during air-assisted spraying. *Biosyst. Eng.* 218, 153–162. <https://doi.org/10.1016/j.biosystemseng.2022.04.003>.